Brownian Dynamics Simulation of Hyperbranched Polymers under Elongational Flow

Igor M. Neelov and David B. Adolf*

Department of Physics and Astronomy, University of Leeds, Leeds LS2 9JT, United Kingdom

Received: August 20, 2003

Brownian dynamics simulations of trifunctional hyperbranched polymers (HP) of different molecular weight (N), degree of branching (DB), and Wiener index (W) have been performed under the influence of uniaxial elongational flow. Perfect trifuctional dendrimers with a trifunctional core up to the sixth generation were also studied for comparison. A freely jointed bead-rod model with excluded volume and hydrodynamic interactions has been used. The dependence of conformational properties and the intrinsic elongational viscosity on the flow rate were obtained. It was shown that both the degree of branching and the Wiener index significantly influence the conformational properties and the elongational viscosity of the molecules at all elongational rates. The coil−stretch transition was observed for all hyperbranched polymers with it being less pronounced than a linear polymer chain but more pronounced than a perfect dendrimer. Findings reveal that critical elongational rate scales as W^{-3}. The dependence on N is weak and is not described by a power law. The orientation and the deformation of the HP is observed to occur in two stages as it was for a linear polymer and a dendrimer with a bifunctional core. The molecule first orients at low flow rate as a whole along the flow axis without significant deformation and local orientation. Increasing flow rate leads to local orientation on the level of the monomer and to significant global deformation of the molecule which plateaus at high flow. At high elongational flow rates, both the plateau value of the average squared radius of gyration and the plateau value of the elongational viscosity scale as approximately W^3. The dependence of these values on N is centered around $N^{0.48}$ and $N^{0.94}$ correspondingly. The ratio of $\langle R_g^2 \rangle / [\eta_{el}]$ does not change significantly but passes through a small and broad maximum during the transition.

I. Introduction

Dendritic tree-like polymers[1] have been intensively studied over the last twenty years due to their unusual properties in comparison with linear polymers. Dendritics adopt a wide range of structures ranging from a completely branched starlike topology (i.e. dendrimers) to much less symmetric arrangements which are composed of a mixture of branched and unbranched monomers (i.e. hyperbranched polymers, HPs). For a given number of monomers, the dendrimer structure is unique whereas a wide range of hyperbranched structures are possible due to the various possible ways of distributing the branched and unbranched monomers. The syntheses of HPs of varying chemistries are present within the scientific literature. For example, Kricheldorf et al.,[2] Hawker et al.,[3] Turner et al.,[4] and Johansson et al.[5] have addressed HP polyesters. Kim and Webster have synthesized HP polyphenylenes[6] and Uhrich et al. have synthesized HP polyethers,[7] in addition to the efforts of Chu and Hawker using HP poly(ether ketones).[8] HP polyurethanes,[9] polycarbosiloxanes,[10] polycarbosilanes,[11] and polyamidoamines[12] have also been considered. Members of these families of materials have been earmarked as thermoset resins[4] and toughening agents,[13] in addition to applications involving drug delivery, viscosity modification, and nonlinear optics.[14]

Whereas a significant amount of experimental research into the rheological properties of branched polymers has concentrated on long-chain branched systems, a limited amount of data for short branched dendritic systems such as dendrimers and HP[15−18] exists within the literature. Dendritics have been shown to reveal an intrinsic viscosity that peaks as a function of molecular weight in contrast to their linear cousins which exhibit a steady increase of intrinsic viscosity with increasing molecular weight.[19,20] This characteristic has sparked interest for a greater insight into the behavior of materials such as HPs within hydrodynamic fields. Computational efforts such as those due to Mansfield and Klushin[21] using the variational approach of Fixman[22] also revealed intrinsic viscosities which peak with molecular weight. Aerts[23] studied the intrinsic viscosities of a series of dendrimers, hyperbranched, branched, and linear polymers, using a bead model that was an extension of the Muthukumar model which allowed the extent of branching to be varied considerably. The calculated dendrimer and HP intrinsic viscosities did exhibit peaks with the peak for the former being at lower levels of intrinsic viscosity and at higher molecular weights relative to the latter. Widmann and Davies[24] considered phantom chain HPs generated from the iterative addition of AB_2 monomers to a trifunctional B_3 core where A−B is the branching reaction. They varied the reaction probability for the attachment of an A group to the first and the second B group of a given AB_2 monomer. The resulting structures were classified according to the degree of branching (i.e. DB) in addition to the distribution of branched sites (i.e. the Wiener index, W). Intrinsic viscosities determined from computed radii of gyration were observed to peak. Lyulin et al.[25] performed Brownian dynamics simulation of conformational properties of unperturbed HP and rheological properties of HP in shear flow. It was revealed that conformations of HPs under shear flow are very anisotropic. Shear thinning was observed and it was revealed that the zero shear rate HP intrinsic viscosity exhibited a maximum in its dependence on molecular weight. A more detailed analysis of HP shear behavior due to Sheridan et al.[26] used Brownian dynamics and HPs of different molecular weight, degree of branching,

10.1021/jp030994q CCC: $27.50
Published on Web 05/12/2004

and Wiener index. In particular, HPs with the same DB values but with different *W* values were prepared. It was shown that DB alone is not sufficient to characterize HPs since intrinsic viscosity differences between HPs with the same molecular weight and DB but different *W* values could be greater than intrinsic viscosity differences between HPs with the same molecular weight but different DB values.

This current effort applies the Brownian dynamic simulation technique to study the behavior of HPs within a stationary elongational flow. It is well-known that when an elongational flow rate, $\dot{\epsilon}$, that is imposed on a flexible linear polymer chain in dilute solution exceeds a critical value, $\dot{\epsilon}_c$, the chain undergoes a sharp transition from a coil to a stretched state (i.e. the coil−stretch transition).[27,28] This phenomenon has been observed for a host of chains with chemically different backbones including various conformations of a single DNA molecule as presented in the recent works of Perkins, Smith, and Chu.[29,30] Theoretical efforts of these systems due to de Gennes[31] in addition to those due to Hinch[32] revealed the transition may be continuous or discontinuous. The computation efforts of Magda et al.,[33] López et al.,[34] Cifre et al.,[34] Agarwal et al.,[35] and Neelov et al.[36] have also addressed this transition. The efforts of de la Torre et al. on bead-spring models and Neelov et al. on bead-rod models reveal the dependence of $\dot{\epsilon}_c$ on the chain length, *N*, are well described by a power law with exponents of close to 2 and 1.5 for systems performed in the absence and presence of HI, respectively, in good agreement with theoretically predicted values based on the Rouse and Zimm models, respectively.

At present, there are very few if any complementary experimental or computational efforts dealing with the elongational flow behavior of dendrimers and hyperbranched polymers. Lee and McHugh[37] suggested a simplified coarse-grained model of a dendrimer and an HP and employed it within BD simulations in the presence of a shear flow. A limited amount of uniaxial elongational flow data for the dendrimer was also reported in this study. Within these efforts, all monomers belonging to a given generation are replaced by one larger monomer with HI accounted for through the Oseen−Burgers tensor. It was observed that the extensional viscosity for dendrimers of generation numbers 0 through 6 increased with flow. However, the magnitude of this increase was small in comparison with that of linear chains.

A more extensive BD study of the elongational flow behavior of a bead-rod model of a dendrimer incorporating both hydrodynamic interactions (HI) and excluded volume (EV) has recently been performed by the authors of this paper.[36] The behavior of a dendrimer with a bifunctional core and trifunctional branching points was studied at different elongational flow rates with the number of generations varying from 2 to 6. Similar to linear chains, the orientation and the deformation of the HP was observed to occur in two stages for all the dendrimers studied. However, the magnitude of the transition was less pronounced with the dendrimers exhibiting a smaller final degree of extension over a larger window of elongational flow rate relative to their linear cousins. Additionally, the molecular weight dependence of the onset of the transition was significantly weaker than that for the linear systems and could not be described by a power law.

The Brownian dynamics of free-draining HPs without excluded volume interactions were reported by Lee and McHugh.[38] The HPs consisted of rigid trumbbells and flexible linear Fraenkel spring units. Shear and some elongational flow data were reported for several HPs where the number of spring units between trumbbells was varied. For small elongational flow rates, the HPs were observed to obey Trouton's rule where the elongational viscosity is three times the intrinsic shear viscosity as expected within the linear regime. At high elongational flow rates, the ratio of the elongational to shear viscosity increases significantly but does not plateau as the model does not take into account the finite extensibility of the HP monomers.

This paper carries on with the authors' earlier computational investigations of dendrimers under elongational flow by studying the elongational flow behavior of a wide range of trifunctional hyperbranched polymers. A bead-rod model with explicit HI and EV is employed. In Section II, further details of the invoked model and the simulation algorithm are presented. Results are presented in Section III which reveal the onset of coil−stretch transition depends essentially on the Wiener index *W* and weakly on the number of monomers in the HP. The ratio $\langle R_g^2\rangle/[\eta_{el}]$ is observed not to change significantly during the transition. Conclusions are presented in Section IV.

II. Model and Algorithm Details

A. Simulation Algorithm. Brownian dynamics simulations of hyperbranched polymers and dendrimers with trifunctional cores and trifunctional branching points in the presence of elongational flow have been performed. Monomers are represented by beads with a friction coefficient ζ. Beads are connected by rigid rods of length *l* and the total number of monomers for a given HP or dendrimer is denoted by *N* where *N* is 94, 190, or 382 corresponding to the number of monomers within trifunctional dendrimers of generation 4, 5, and 6, respectively. Torsional and valence angle potentials are not employed. At each integration step, a two-stage procedure was used to generate the new coordinates. First, the unconstrained displacement was calculated by using the Ermak−McCammon equation of motion[39]

$$\vec{r}_i = \vec{r}_i^{\,0} + \frac{\Delta t}{kT}\sum_j \mathbf{D}_{ij}^{\,0}\cdot\vec{F}_j^{\,0} + \vec{v}_i^{\,0}\cdot\Delta t + \vec{\Phi}_i^{\,0}(\Delta t) \qquad i = 0, ..., N \tag{1}$$

where $\vec{r}_i^{\,0}$ is the position vector for bead *i* before a Brownian dynamics step, Δt. The core bead is labeled as $i = 0$. *k* is Boltzmann's constant and *T* is the simulation temperature. $\mathbf{D}_{ij}^{\,0}$ is the diffusion tensor, $\vec{F}_j^{\,0}$ is the force on bead *i* arising from bead *j*, and $\vec{v}_i^{\,0}$ is the velocity of the solvent at the position of bead *i*. For the steady elongational flow studied here $v_{i,x}^{\,0} = x_i^0\dot{\epsilon}$, $v_{i,y}^{\,0} = -0.5y_i^0\dot{\epsilon}$, and $v_{i,z}^{\,0} = -0.5z_i^0\dot{\epsilon}$. The solvent is represented as a structureless continuum with chain-solvent collisions mimicked by the vector $\vec{\Phi}_i^{\,0}$, which has a zero mean and a variance-covariance matrix given by

$$\langle\vec{\Phi}_i^{\,0}(\Delta t)\vec{\Phi}_j^{\,0}(\Delta t)\rangle = 2\Delta t\mathbf{D}_{ij}^{\,0} \tag{2}$$

The constraint forces are computed within the second stage of an integration step in a fashion suggested by Öttinger[40] with a relative tolerance of 2×10^{-6}. The Lennard-Jones potential

$$U_{LJ} = \sum_{ij} 4\epsilon\left(\left(\frac{\sigma}{r_{ij}}\right)^{12} - \left(\frac{\sigma}{r_{ij}}\right)^{6}\right) \tag{3}$$

is invoked between all nonbonded beads *i* and *j* with a cutoff distance, r_{cutoff}, of 2.5σ. The parameters $\sigma = 0.8l$ and $\epsilon = 0.3kT$ were used following Rey et al.[41] and the authors' previous efforts with linear chains and bifunctional cored dendrimers in elongational flow.[36] HI are represented rigorously by means of the

Rotne−Prager−Yamakawa interaction tensor[42] with off-diagonal elements given by eqs 4a and 4b. For the case of nonoverlapping beads (i.e. when $R_{ij} = |\vec{R}_{ij}| = |\vec{r}_i - \vec{r}_j| \geq 2a$) one has

$$D_{ij}^{\alpha\beta} = h^*\left(\frac{\pi}{3}\right)^{1/2}\left(\frac{3kT}{4\zeta}\right)\left(\frac{l}{R_{ij}}\right)\left[\left(\delta_{\alpha\beta} + \frac{R_{ij}^{\alpha}R_{ij}^{\beta}}{R_{ij}^{2}}\right) + \frac{2a^2}{3R_{ij}^{2}}\left(\delta_{\alpha\beta} - \frac{3R_{ij}^{\alpha}R_{ij}^{\beta}}{R_{ij}^{2}}\right)\right] \quad (4a)$$

where R_{ij} is the separation between beads i and j each with Stokes' hydrodynamic radius a. α and β represent the x, y, or z components of the vector $\vec{R}_{ij}$. The strength of the HI is set by the parameter $h^* = (3/\pi)^{1/2}a/l = (3/\pi)^{1/2}\zeta/(6\pi\eta_s l)$, where η_s represents the solvent viscosity. A value of $h^* = 0.25$ is employed due to its success within earlier studies using a bead-spring model[34] and a bead-rod model.[36] This h^* value corresponds to a hydrodynamic radius, a, of $0.257l$. Due to the use of soft intermolecular potentials the beads can overlap (i.e. $R_{ij} < 2a$). In this case

$$D_{ij}^{\alpha\beta} = (kT/\zeta)\left[\left(1 - \frac{9R_{ij}}{32a}\right)\delta_{\alpha\beta} + \left(\frac{3}{32a}\right)\frac{R_{ij}^{\alpha}R_{ij}^{\beta}}{R_{ij}}\right] \quad (4b)$$

In this paper, dimensionless quantities are used where length (l), energy (kT), and translational friction ($\zeta = 6\pi\eta_s a$ of chain beads where η_s represents the solvent viscosity) are set to unity. It follows that time is scaled by $\zeta l^2/kT$ and elongational rate by $kT/\zeta l^2$. Any physical quantities within the remainder of this paper are scaled by these units unless otherwise indicated. Elongational rates spanning a range from 0.0001 to 10 and a time step between $\Delta t = 3 \times 10^{-4}$ and 5×10^{-5} are used within this investigation. An equilibration period of 2.5×10^6 to 2.5×10^7 time steps, depending on the number of monomers and elongational rate, was performed before trajectories were saved for analysis. The achievement of steady-state conditions was monitored through the radius of gyration, R_g, the components of the inertia tensor, **T**, and the average distance from the core of the dendrimer to the groups located on its periphery. Following equilibration, production runs were performed and the resulting trajectories analyzed. Each production run was between 5×10^6 and 5×10^7 time steps in length depending on N, the elongational rate, and the magnitude of the time step. Error bars for all plotted data points are smaller than the size of the symbol used unless otherwise indicated. Furthermore, lines connecting data points within figures are an aid to the eye unless otherwise indicated.

B. Preparation of Initial Structures and Conformations of Hyperbranched Polymers. The fully branched structure of a dendrimer with a given number of monomers is unique. This is not the case for a hyperbranched molecule where the extent of unbranched character and the location within the molecule of the branching points can be varied while the number of monomers is held fixed. The extent of unbranched content within a hyperbranched molecule is characterized by the degree of branching, DB. The general distribution of branched and unbranched points within a hyperbranched molecule can be characterized by the Wiener index, W. In greater detail, DB is defined for all molecules according to Holter et al.[43]

$$\mathrm{DB} = \frac{2D}{2D + L} \quad (5)$$

D is the number of fully branched ("dendritic") beads and L is the number of partially reacted ("linear") beads. The Wiener index is defined by the formula,

$$W = \frac{1}{2}\sum_{j=1}^{N}\sum_{i=1}^{N} d_{ij} \quad (6)$$

where d_{ij} is the number of bonds separating the beads i and j of the structure, counted along the shortest path between them. The index was introduced by Wiener in 1947[44] and was found to correlate with the boiling points of alkanes. Since then, it has been found to correlate closely with bulk refractive index, density, viscosity, melting point, boiling point, and surface tension of hydrocarbons,[45,46] specific π-electronic energies, and energy gaps of conjugated polymers. W also correlates reasonably with the specific rotation of various chain chemistries with vinyl additions and has been linked to the surface-to-volume ratio of molecules, implying a further correlation with molecular interaction.[47,48]

The dendrimers and hyperbranched molecules within this study were initially generated by a procedure suggested by Widmann and Davies[24] and are the same structures employed within the authors' previous efforts illustrating the W and N dependence of the shear intrinsic viscosity of dendrimers and hyperbranched polymers.[26] Examples of the topological structures employed are given in Figure 1 for the $N = 190$ family. The structures within Figure 1 are meant to reflect only their general topology. The real space representations of these structures are more compact coils in the absence of flow. Further details behind the generation of the initial structures are found within the paper of Widmann and Davies.[24]

As mentioned previously, the HP within this study have $N = 94$, 190, or 382 monomers corresponding to the number of monomers within their dendrimer cousins of generations 4 through 6. Following Sheridan et al.,[26] large populations of 5×10^6 to 1×10^7 HP structures with varying W values were generated at each combination of N and DB values. The DB values employed within this study are 0.4, 0.6, and 0.8. The probability distributions for these populations at fixed N and DB adopt a Gaussian shape when plotted as a function of W. In this study, two structures from each population were chosen where each structure has one-fourth the probability of occurrence of the peak structure. For each distribution, one structure has a W value lower than the W value of the peak structure (i.e. the left one-fourth maximum, LFM) while the second structure possesses a W value higher than the W value of the peak structure (i.e. the right one-fourth maximum, RFM). At fixed N and DB, the LFM structure is more compact than the corresponding RFM structure. Data for these structures will be denoted by filled (LFM) or open (RFM) symbols respectively in all plots unless otherwise indicated. The symbol shapes of circle, triangle, and square are assigned to DB = 0.4, 0.6, and 0.8 data, respectively, on all further figures. Trifunctional dendrimer data are represented by diamonds.

III. Results and Discussion

A. Characteristics of Dendrimers and Hyperbranched Polymers in the Absence of Elongational Flow. The N dependence of the mean squared radius of gyration in the absence of flow, $\langle R_g^2\rangle_0$, is shown in Figure 2 for hyperbranched polymers with a degree of branching DB = 0.4 and 0.8. Similar data for the trifunctional dendrimer are also shown as diamonds. All lines are best fits to the data. It is observed that the dendrimer at each N value has the smallest $\langle R_g^2\rangle_0$, while the corresponding DB = 0.4 RFM hyperbranched molecule possesses the largest

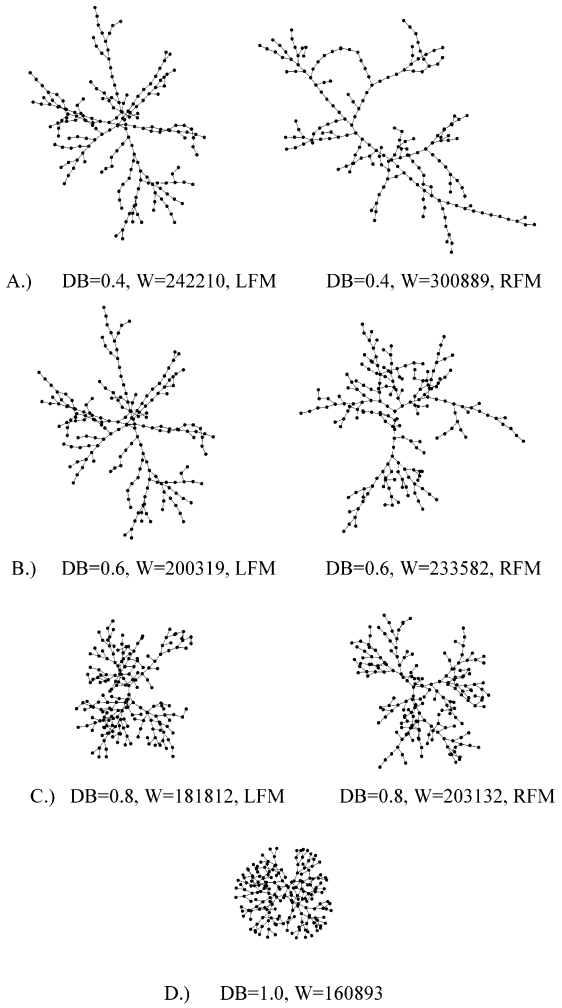

Figure 1. Examples of some of the hyperbranched polymers and the trifunctional dendrimers employed within the study. The structures correspond to the $N = 190$ family at the degrees of branching of (A) DB = 0.4, (B) 0.6, (C) 0.8, and (D) 1.0 (dendrimer). Each structure's Wiener index value is also given. Hyperbranched structures are labeled as to whether they correspond to LFM or RFM representations (see text).

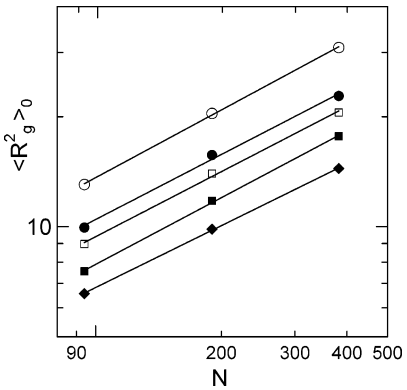

Figure 2. The N dependence of the mean squared radius of gyration in the absence of flow, $\langle R_g^2\rangle_0$, of an HP with DB = 0.4 (circles) and DB = 0.8 (squares) in addition to that for a trifunctional dendrimer (diamonds). Solid lines are best fits in each case. Filled and open symbols denote LFM and RFM structures, respectively.

$\langle R_g^2\rangle_0$. The data for all structures are observed to be consistent with a power law with a best fit exponent (i.e. slope on the log−log scale) in the range of 0.57 ± 0.03 to 0.62 ± 0.03. The values of these exponents are in close agreement with previous results for bifunctional cored dendrimers [36] (i.e. slope of 0.60) and the results of Lyulin et al.[25] (i.e. slope of 0.62*)* for the same trifunctional cored dendrimers and the same model as within this study. Earlier MD simulations due to Murat and Grest[49] of dendrimers with a trifunctional core also revealed values of this exponent to be between 0.59 and 0.61. The dependence of $\langle R_g^2\rangle_0$ on Wiener index W (not shown) is close to $\sim W^{1.0}$ for unperturbed structures (i.e without flow or at very small flow fields) in accordance with results obtained earlier by Sheridan et al.[26]

More detailed insight into the dendrimer's and HP's internal structure is available through the radial distribution functions generated from all monomers. Panels A and B of Figure 3 reveal the distribution of monomers around the center of mass for the $N = 190$ dendrimer and the corresponding LFM and RFM HPs at DB values of 0.4 and 0.8. A dip in the distribution for the dendrimer (line 1 on Figure 3A,B) between r values of 1 and 2 is observed. The LFM HPs (Figure 3A) do not reveal similar dips with the DB = 0.8 illustrating a plateau between r values of 1 and 2 and the DB = 0.4 data exhibiting a distribution function that steadily decreases as the distance from the core increases. Both RFM HPs with DB values of 0.4 and 0.8 illustrate a distribution function that steadily decreases with no sign of any dips or plateaus. The decay in these functions is slower for HPs with lower DB values as these structures are less compact relative to their high DB cousins. This also is true when comparing RFM HPs to LFM HPs at the same N and DB values.

Figure 3C depicts Kratky plots for the $N = 190$ LFM and RFM HPs with DBs of 0.4 and 0.8 in addition to the corresponding trifunctional dendrimer. The solid line represents data for a sphere with a radius of gyration equal to that for the $N = 190$ dendrimer. The second maximum observed in the Kratky plot for the sphere is clearly observed within the corresponding plot for the dendrimer while its presence is suggested within the plot for the LFM DB = 0.8 HP. Lower DBs and RFM structures tend to deviate the most from the sphere's Kratky plot as expected due to the less compact and more sprawled out nature of these structures. The observed differences in plots comprised of opened (RFM) and filled (LFM) symbols of the same sort attest to the importance of the W value in characterizing HP statistical properties

B. Characteristics of Dendrimers and Hyperbranched Polymers under Elongational Flow. *i. Elongational Rate Dependence of Chain Size.* $\langle R_g^2\rangle$ is plotted in Figure 4a as a function of the elongational flow rate for $N = 382$ HPs with different DB and W values in addition to the associated $N = 382$ trifunctional cored dendrimer. The magnitude of the transition is the largest for the more sprawled out structures (i.e. RFM low DB HP structures, open circles) and the smallest for the dendrimer (i.e. diamonds). The maximum extended length of an HP or dendrimer is significantly less than that observed in the authors' previous efforts[36] with the elongational flow behavior of linear chains with the same value of N (not shown) due to connectivity and congestion issues. These observed HP transitions are also significantly broader than for a linear chain in elongational flow (not shown). The transition region for an HP or a dendrimer consisting of $N = 190$ monomers spans nearly two decades of $\dot{\epsilon}$ (i.e., $\dot{\epsilon} = 0.1$ to 10) in comparison with approximately one decade for a linear chain of a similar molecular weight. Additionally, the onset of the transition for HPs is observed to occur at lower $\dot{\epsilon}$ values relative to the dendrimer but at higher $\dot{\epsilon}$ than for a linear chain with the same number of monomers (not shown).

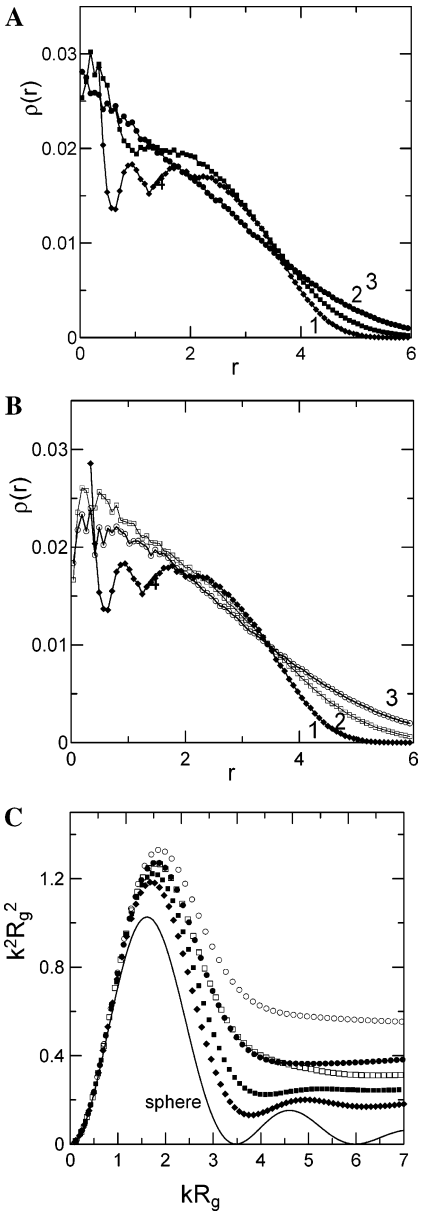

Figure 3. (A) The radial distribution function of bead positions relative to the center of mass for the $N = 190$ dendrimer (diamonds, 1), the $N = 190$ LFM HPs with DB = 0.8 (squares, 2) and DB = 0.4 circles (3) without flow; (B) the same for the $N = 190$ dendrimer (1) and $N = 190$ RFM structures with DB = 0.8 (2) and 0.4 (3). (C) The Kratky plot for the $N = 190$ LFM HPs with DB = 0.4 (filled circles), DB = 0.8 (filled squares) and the $N = 190$ RFM HPs at DB = 0.4 (open circles), DB = 0.8 (open squares) in the absence of flow. The $N = 190$ dendrimer data are also plotted as diamonds.

The plateau values of the mean squared radius of gyration at high elongational rate, $\langle R_g^2\rangle_{max}$, are plotted in Figure 4B as a function of N on a log−log scale for the dendrimer in addition to LFM and RFM HP structures with DB values of 0.4 and 0.8. Best fit solid lines are drawn through each set of data. The slope of the best fit line for the dendrimer data is 0.40 ± 0.04. The corresponding slope for the LFM DB = 0.8 HP data is 0.44 ± 0.05 and that for the RFM DB = 0.4 HP data is 0.50 ± 0.05. Structures with intermediate values of DB and W (not shown) have slopes that lie between 0.44 and 0.50.

$\langle R_g^2\rangle_{max}$ is plotted in Figure 4c as a function of Wiener index W on a log−log scale for three families composed of $N = 94$, 190, and 382 beads. Each family is comprised of the dendrimer and six HP structures (i.e., LFM and RFM at DB values of 0.4, 0.6, and 0.8). The slope of the best fit line through each data set is nearly 3 in all cases (i.e. the values are between 2.93 ± 0.07 and 3.04 ± 0.07 for N between 94 and 382). This dependence can be compared with the scaling of $\langle R_g^2\rangle_0$ as $W^{1.0}$ for unperturbed structures (i.e. without flow or at very small flow fields) to reveal the influence of the Wiener index on $\langle R_g^2\rangle$ is much stronger in the extended state than in the unperturbed state. This behavior of $\langle R_g^2\rangle_{max}$ on N and W will be compared with the similar behavior for the plateau intrinsic elongational viscosity at high elongational rates later in this paper.

ii. Elongational Rate Dependence of HP and Dendrimer Shape. The average shape of the HPs and the dendrimer as a whole under uniaxial elongational flow can be further characterized quantitatively by components of the mean squared radius of gyration in the direction of the flow, $\langle R_{gx}^2\rangle$, and perpendicular to the direction of flow. The behavior of $\langle R_{gx}^2\rangle$ as a function of flow rate was observed to be similar to that illustrated in Figure 4A for $\langle R_g^2\rangle$ and hence is not shown. As the y and z projections are practically indistinguishable, only $\langle R_{gz}^2\rangle$ data are presented in Figure 4D for $N = 190$.

At small elongational rates, (i.e., $\dot{\epsilon} < 0.01$) $\langle R_{gz}^2\rangle = \langle R_g^2\rangle/3$ and equal to the unperturbed values. The values of $\langle R_{gz}^2\rangle$ decrease and approach values nearly 10 times less than values at low flow rates. However, this decrease of $\langle R_{gz}^2\rangle$ for the HP and dendrimers is not as dramatic as that observed for linear chains.[36] Comparing panels A and D of Figure 4 reveals the onset of the transition occurs at lower $\dot{\epsilon}$ for $\langle R_{gz}^2\rangle$ (and also for $\langle R_{gx}^2\rangle$ which is not shown) than for $\langle R_g^2\rangle$ as is also observed in an earlier work for linear chains and bifunctional cored dendrimers.[36] This signifies the initial response of the HPs and dendrimer molecules is an alignment of the molecule as a whole along the flow direction at low flow. As elongational flow is further increased, deformation of the molecule through increased local orientation occurs as will be illustrated in the next section.

iii. Local Orientation of HP and Dendrimer. The local orientation of the monomers of the HPs and the dendrimer at different elongational rates can be characterized by using a local orientational angle, θ_x, representing the average angle between unit vectors along the individual rigid bonds of the HP or dendrimer and the flow direction. The quantity $\langle\cos^2\theta_x\rangle$ is plotted within Figure 5 for $N = 190$ LFM and RFM HP structures with DB values of 0.4 and 0.8. The $N = 190$ dendrimer data are also illustrated. The local orientational transition from randomly oriented bonds (i.e. $\langle\cos^2\theta_x\rangle = 1/3$) to highly oriented bonds (i.e. $\langle\cos^2\theta_x\rangle$ approaching 1) occurs at a larger $\dot{\epsilon}$ value than observed for the radius of gyration for dendrimers and HPs with the same number of monomers, N. This implies different values of $\dot{\epsilon}_c$ would be predicted depending on whether the onset of the coil−stretch transition was detected with use of $\langle\cos^2\theta_x\rangle$ (e.g. via birefringence data) or via global orientation. It is noticed that the orientations of the DB = 0.4 LFM and RFM HPs start at different elongational rates but reach similar degrees of orientation at high flows.

iv. Radial Distribution Function of Internal and Terminal Monomers. Figure 6A illustrates the elongational flow rate dependence of the density distribution function, $\rho(r)$, of monomers for the $N = 190$ LFM HP with a DB value of 0.4 where r is the distance from the center of mass. $\rho(r)$ data at small elongational rates (i.e. line 1) are qualitatively similar to thase in the absence of flow (Figure 3A). At higher rates which correspond to the coil−stretch transition region, this distribution becomes broader with peaks beginning to appear at various positions along the curve (lines 2 and 3) which sharpen with further increases in flow rate. However, the peaks for these

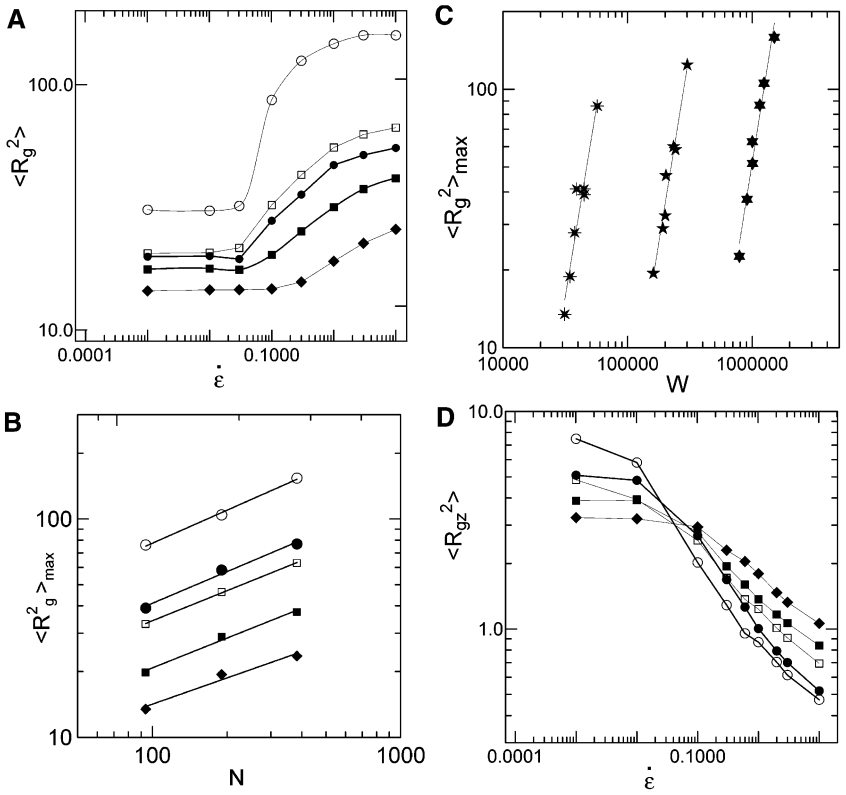

Figure 4. (A) The elongational flow rate dependence of $\langle R^2_g \rangle$ for $N = 382$ HPs with different DB and W values along with similar data for the associated $N = 382$ dendrimer. Filled and open symbols denote LFM and RFM structures, respectively. (B) The N dependence of $\langle R_g^2 \rangle_{max}$ for LFM and RFM HPs at DB values of 0.4 and 0.8 along with the associated dendrimer. Filled and open symbols denote LFM and RFM structures, respectively. (C) The W dependence of $\langle R_g^2 \rangle_{max}$ for three families of molecules. Each family has members with the same number of beads (i.e. $N = 94$, 190 and 382 are denoted as four-pointed, five-pointed, and six pointed stars, respectively) and is composed of a dendrimer in addition to six HP structures corresponding to RFM and LFM structures at DB values of 0.4, 0.6, and 0.8. Note that symbols within this plot are differentiating by N value only. (d) The elongational flow rate dependence of the component of the mean squared radius of gyration perpendicular to flow, $\langle R_{gz}^2 \rangle$, for the $N = 190$ HP with DB = 0.4 (open and filled circles) and DB = 0.8 (open and filled squares) in addition to the $N = 190$ trifunctional dendrimer (diamonds). Filled and open symbols denote LFM and RFM structures, respectively.

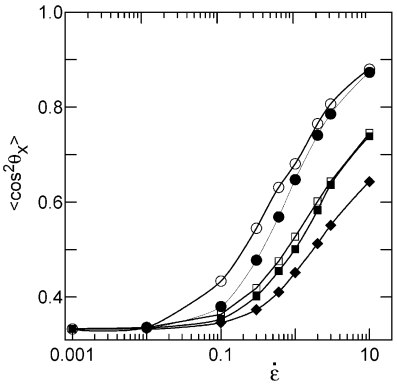

Figure 5. The elongational flow rate dependence of the local orientation of monomers, $\langle \cos^2\theta_x \rangle$, for $N = 190$ LFM and RFM HPs with DB values of 0.4 and 0.8 in addition to that for the corresponding $N = 190$ trifunctional dendrimer. Filled and open symbols denote LFM and RFM structures, respectively.

trifunctional systems are not as pronounced as the peaks observed previously for bifunctional dendrimers.[36] It is felt that this is due to the bifunctional cored dendrimers being axially symmetric at high flow (i.e. at complete elongation) while the trifunctional HPs and trifunctional dendrimers are asymmetric at high flow.

v. Distribution Function of Gyration Radius. Figure 6B reveals the distribution function of the values of the radius of gyration $\rho(R_g)$ for the same $N = 190$ HP (DB = 0.4, LFM) at different elongational rates labeled 1 (lowest rate) through 8 (highest rate) on the figure. At elongational flow rates corresponding to the coil−stretch transition, $\rho(R_g)$ broadens and shifts to high R_g values. The increased width of the distribution in this region reflects an increase in the fluctuations of the HP's size in the vicinity of the transition. Similar broadening within the transition region was obtained earlier for a linear chain and a dendrimer with a bifunctional core.[36] Further increases in flow rates narrows $\rho(R_g)$ and shifts it to higher R_g values whereby it approaches its maximum plateau value, $R_{g,max}$.

vi. Scattering Factor of Dendrimer in Flow. Values of the static structure factor $S(k)$ for wave vectors directed along the flow, $S(k_x)$, and perpendicular to the flow, $S(k_z)$, were calculated at different values of flow rate. Examples of such plots are illustrated in Figure 7, panels A and B, for the $N = 190$ LFM HP with a DB of 0.4. It is observed that the initial slope of $S(k_x)$ (Figure 7A) increases with increasing flow while the slope of $S(k_z)$ (Figure 7B) decreases with increasing flow. This result is in good agreement with the observed increase of $\langle R_{gx}^2 \rangle$ and the decrease of $\langle R_{gz}^2 \rangle$ with increasing flow.

vii. Snapshots of the Dendrimer. Snapshots of the $N = 190$ and DB = 0.4 LFM HP and its dendrimer cousin at different elongational rates are presented in Figure 8, panels A through C. Light beads within all of these pictures represent terminal monomer units. For the dendrimer, these correspond to the monomers of the last generation while for HP polymers they are at different positions on the HP connectivity tree. Figure 8A shows the conformation at an elongational flow rate of $\dot{\epsilon} = 0.01$ before the coil−stretch transition. At higher flow rates near

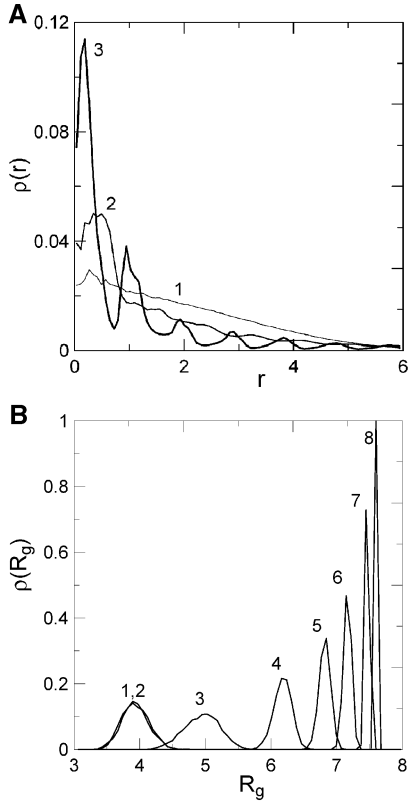

Figure 6. (A) The radial distribution function of bead positions relative to the center of mass for the $N = 190$ LFM HP with a DB = 0.4 at $\dot{\epsilon} = 0$ (1), 0.6 (2), and 3 (3). (B) The distribution function for the radius of gyration of the $N = 190$ LFM HP with a DB = 0.4 at the flow rates $\dot{\epsilon} = 0$ (1), 0.01 (2), 0.1 (3), 0.3 (4),0.6 (5), 1 (6),3 (7), and 10 (8).

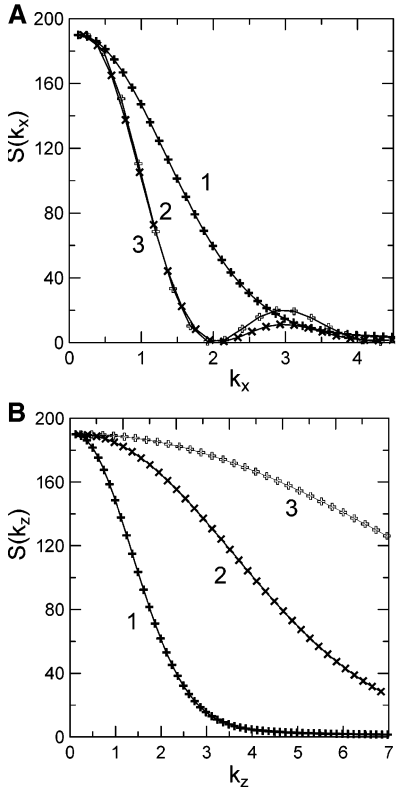

Figure 7. (A) The static structure factor for the $N = 190$ LFM HP with a DB of 0.4 in the direction of flow at the elongational flow rates $\dot{\epsilon} = 0.0$ (1), 0.3 (2), and 10.0 (3) . (B) The static structure factor for the same HP perpendicular to the flow at the same elongational flow rates as in part a.

the middle of the coil−stretch transition, Figure 8B reveals the molecules become oriented along the direction of flow and are more anisotropic. The anisotropy increases as the flow rate increases further as seen within Figure 8C. Figure 8C corresponds to an elongational flow rate close to that for the state of maximum extension. These observations give further insight into the flow induced formation of peaks within the density distribution functions depicted in Figure 6A. Increasing flow rate leads to a more regular distribution of chain monomers along the flow axis (see maxima on Figure 6A) for both the HPs and the trifunctional dendrimers. However, the extent of this regularity is not as pronounced for the trifunctional dendrimers in comparison to what was seen in an earlier publication for bifunctional dendrimers.

viii. Elongational Viscosity. The primary rheological property of interest in this study is the stress tensor, given by the Kramers expression

$$\tau = -\eta_0 \underset{\sim}{\dot{\epsilon}} - n\langle \mathbf{RF} \rangle + n\mathbf{I} \tag{7}$$

where $\underset{\sim}{\dot{\epsilon}}$ is the rate-of-strain tensor and η_0 is the elongational viscosity of the solvent. For simple elongational flow, $\dot{\epsilon}_{xx} = -2\dot{\epsilon}_{yy} = -2\dot{\epsilon}_{zz} = \dot{\epsilon}$ and all off-diagonal components of the rate-of-strain tensor are zero. n represents the number density and **RF** is the virial tensor for a single molecule. The elongational viscosity is expressed in terms of the elongational stress as

$$\eta_{\mathrm{el}} = -\frac{\tau_{xx} - \tau_{zz}}{\dot{\epsilon}} = \eta_0 + n\frac{\langle \mathbf{R}_x\mathbf{F}_x - \mathbf{R}_z\mathbf{F}_z \rangle}{\dot{\epsilon}} \tag{8a}$$

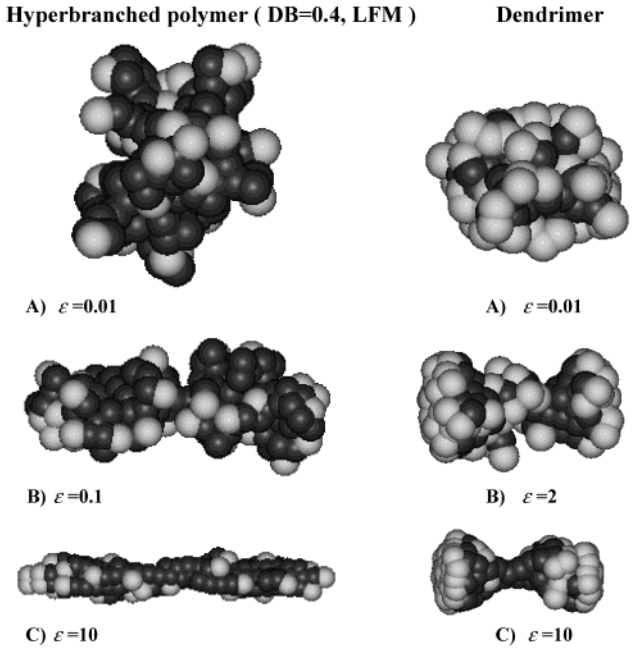

Figure 8. Snapshots of the $N = 190$ with a DB = 0.4 LFM HP and dendrimer from simulations at different elongational flow rates: (A) before the coil−stretch transition, (B) within the transition region, and (C) close to state of maximum extension.

and the corresponding intrinsic elongational viscosity is calculated as

$$[\eta_{\mathrm{el}}] = \left[\frac{(\eta_{\mathrm{el}} - \eta_0)}{n\eta_0}\right] \tag{8b}$$

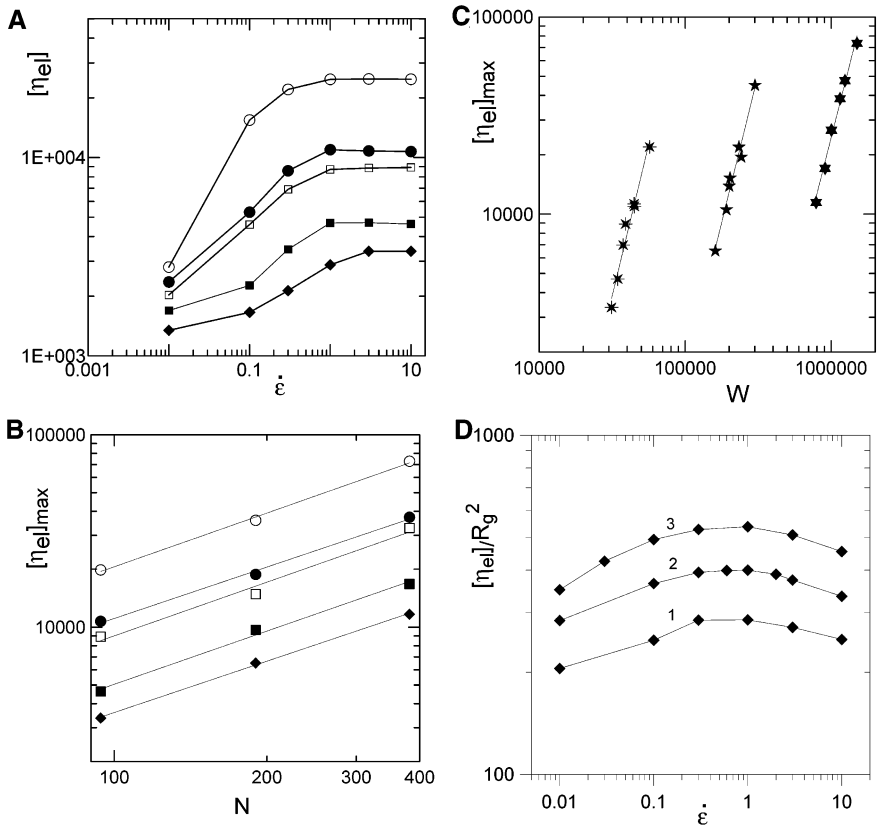

Figure 9. (A) The elongational flow rate dependence of the intrinsic elongational viscosity, $[\eta_{el}]$, for the $N = 94$ RFM and LFM HPs with DB values of 0.4 and 0.8 in addition to the corresponding $N = 94$ dendrimer. Filled and open symbols denote LFM and RFM structures, respectively. (B) The dependence of the plateau values of the intrinsic elongational viscosity, $[\eta_{el}]_{max}$, on the total number of beads within the HP or dendrimer, N. Best fit curves are represented by solid lines. Filled and open symbols denote LFM and RFM structures, respectively. (C) The dependence of the plateau values of the intrinsic elongational viscosity, $[\eta_{el}]_{max}$, on the Wiener index of the HP and dendrimer. Best fit curves are represented by solid lines. Note that symbols within this plot are differentiated by the N value only. (D) The ratio $[\eta_{el}]/\langle R_g^2\rangle$ for dendrimers with $N = 94$ (1), 190 (2), and 382 (3) as a function of elongational flow rate.

The intrinsic elongational viscosity, $[\eta_{el}]$, is plotted in Figure 9A for the $N = 94$ HP polymers with different DB and W values in addition to the associated $N = 94$ trifunctional cored dendrimer as a function of elongational rate. Each set of data reveals a transition from an unperturbed "coil" at low elongational rates to a highly stretched conformation at high elongational rates. Plateau values of $[\eta_{el}]$ at high elongational rates are observed for all HPs and dendrimers studied. HP plateau values are higher than the dendrimer plateau value. The largest plateau value is observed for the DB = 0.4 LFM structure. Furthermore, at a fixed DB value, the plateau value for the RFM structure is higher than that for the corresponding LFM structure. These observations are expected since more compact structures have higher DBs and low W values.

The plateau values of the intrinsic elongational viscosity, $[\eta_{el}]_{max}$, at high elongational flow rates for the $N = 94$, 190, and 382 dendrimers along with the associated HPs with different DB and W values are plotted in Figure 9B versus N on a log−log scale. The best fit lines running through the symbols indicate $[\eta_{el}]_{max} \sim N^a$ where a is in the range of 0.92 ± 0.05 to 0.96 ± 0.05 for N between 94 and 382. This is in contrast to BD simulations of linear chains with HI where $[\eta_{el}]_{max} \approx N^{2.67}$ but comparable to the scaling $[\eta_{el}]_{max} \approx N^{1.0}$ for dendrimers with a bifunctional core obtained by the authors in a previous study.[36]

The plateau values of the intrinsic elongational viscosity at large elongational rates for HPs and trifunctional dendrimers comprised of $N = 94$, 190, and 382 monomers are plotted in Figure 9C versus Wiener index W on a log−log scale. The best fit lines running through the data indicate $[\eta_{el}]_{max}$ scales nearly as W^3 for all N (i.e. the exponents changes between 2.92 ± 0.08 and 3.06 ± 0.08 for N from 94 to 382). These exponents are similar to that obtained for $\langle R_g^2\rangle_{max}$ as a function of W (see Figure 4C) where exponents fell within a window of 2.93 to 3.04. This suggests that the intrinsic elongational viscosity at high elongational flow is proportional to $\langle R_g^2\rangle$.

At low flow rates (i.e. linear regime), it is known that $[\eta_{el}] = 3[\eta_{shear}]$ and Sheridan et al.[26] have revealed a linear dependence between $[\eta_{shear}]$ and $\langle R_g^2\rangle$ via similar BD simulations as within this paper. Therefore, $[\eta_{el}]$ must also be proportional to $\langle R_g^2\rangle$ at small elongational rates in a region where both $[\eta_{el}]$ and $\langle R_g^2\rangle$ are weakly affected by flow. One then may ask whether this proportionality is observed at all elongational flow rates. To check this, the dependence of $[\eta_{el}]/\langle R_g^2\rangle$ on elongational rate $\dot{\epsilon}$ is plotted within Figure 9D for dendrimers with $N = 94$, 190, and 382. It can be seen that this ratio is not constant but does not change significantly during the coil−stretch transition and passes through a broad and small maximum within the transition region. For the HPs, the dependence of this ratio on $\dot{\epsilon}$ is very close to that for the trifunctional dendrimer with the same N value (not shown).

ix. Dependences of Critical Transition Rate on Chain Length N and Wiener Index W. Plots of $\langle R_g^2\rangle$ versus $\dot{\epsilon}$ for each HP and each trifunctional dendrimer studied within $N = 94$, 190, and 382 monomers have been constructed. Figure 4A is an example of such a plot for $N = 382$ with the critical transition rate, $\dot{\epsilon}_c$, being defined as the midpoint of the transition in $\langle R_g^2\rangle$. In Figure 10A, $\dot{\epsilon}_c$ values are plotted versus N revealing that $\dot{\epsilon}_c$ is virtually constant over the studied interval. A comparable result of a weak

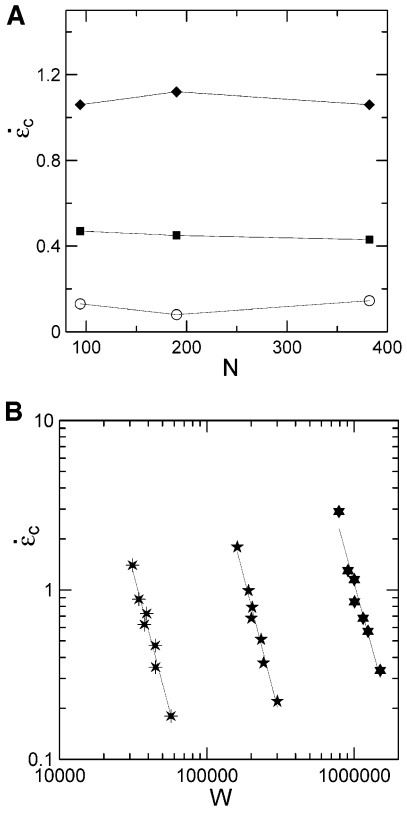

Figure 10. (A) The dependence of the critical value of the elongational flow rate, $\dot{\epsilon}_c$, on the total number of beads within the HP or dendrimer, *N*. Filled and open symbols denote LFM and RFM structures, respectively. (B) The dependence of the critical value of the elongational flow rate, $\dot{\epsilon}_c$, on the Wiener index *W*. Note that symbols within this plot are differentiated by the *N* value only.

dependence of the critical elongational rate on *N* over the similar interval of *N* was obtained by the authors for bifunctional cored dendrimers.[36] In Figure 10B, $\dot{\epsilon}_c$ values are plotted in log−log scale versus the Wiener index *W* at $N = 94$, 190, and 382, respectively. The dependence of $\dot{\epsilon}_c$ on *W* is described well by a power law with an exponent in the region of −3.0 to −3.2 for the different values of *N*. Both $\langle R_g^2\rangle_{max}$ (Figure 4C) and $[\eta_{el}]_{max}$ (Figure 9C) revealed similar magnitudes for their power law scaling exponents with *W* (i.e. near 3). The authors are currently exploring possible explanations for these similarities.

For a linear polymer chain in elongational flow, the value of the critical elongational rate is close to the inverse maximum relaxation time of the chain for situations with or without hydrodynamic interactions (i.e. for the Zimm and Rouse models, respectively). To check whether a similar connection is held for dendrimers and HPs, it is necessary to calculate the maximum relaxation times for these molecules, which will be performed in a forthcoming paper devoted to their internal mobility in elongational flow.

IV. Summary

Brownian dynamics simulations of the statistical and rheological properties of a bead-rod model of HPs and dendrimers with EV and HI under elongational flow have been performed. HPs with different DB and *W* values were studied and compared at different elongational rates. Both the HP and dendrimer average extension and orientation have been calculated as a function of $\dot{\epsilon}$. At high elongational rates, it was shown that the limiting (plateau) mean squared radius of gyration, $\langle R_g^2\rangle_{max}$, scales as $N^{0.40}$ for a dendrimer and $N^{0.44-0.50}$ for an HP both simulated in the presence of hydrodynamic interactions. This is significantly smaller than $N^{1.5}$ for linear polymer chain with hydrodynamic interactions. The limiting (plateau) intrinsic elongational viscosity $[\eta_{el}]_{max}$ for the HP and the dendrimer is also significantly smaller than for linear polymer chain. $[\eta_{el}]_{max}$ for these systems is observed to scale with *N* as $N^{0.92-0.96}$. This is close to the observed *N* scaling dependence for bifunctional cored dendrimers[36] (i.,e. $N^{1.0}$) and quite different from the observed *N* scaling behavior observed for a bead-rod model of a linear polymer chain with EV and HI (i.e. $N^{2.67}$).[36] The dependence of both $\langle R_g^2\rangle_{max}$ and $[\eta_{el}]_{max}$ on Wiener index *W* is close to W^3. Finally, the dependence of the critical elongational rate, $\dot{\epsilon}_c$, on *N* and *W* was calculated for the first time for HPs and trifunctional cored dendrimers in elongational flow. Findings reveal that $\dot{\epsilon}_c$ for these systems is at most weakly dependent on *N* within the interval $N = 94$ to 382. At the same time, there is strong dependence of this value on the Wiener index that is observed to be near W^{-3}.

Acknowledgment. The authors acknowledge the EPSRC for financial support of this study (GR/M64215). This work is partly supported by INTAS 00-00712 and the ESF program SUPERNET. I.M.N. is grateful for partial support to NWO and the Computer Science Centre (CSC, ESPOO, Finland) for computer time on the parallel SGI Origin 2000 and IBM SC computers.

References and Notes

(1) Flory, P. *Principles of Polymer Chemistry*; Cornell University Press: Ithaca, New York, 1953.
(2) Kricheldorf, H. R.; Zhang, O.; Schwarz, G. *Polymer* **1982**, *23*, 1820.
(3) Hawker, C. J.; Lee, R.; Frechet, J. M. *J. Am. Chem. Soc*. **1991**, *113*, 4583.
(4) Turner, S. R.; Voit, B. I.; Mourey, T. *Macromolecules*. **1993**, *26*, 4617.
(5) Johansson, M.; Malmstrom, E.; Hult, A. *J. Polym. Sci*. **1993**, *A31*, 619. Johansson, M.; Malmstrom, E.; Hult, A. *Macromolecules* **1995**, *28*, 1698.
(6) Kim, Y. H.; Webster, O. *Macromolecules* **1992**, *25*, 5561.
(7) Uhrich, K. E.; Hawker, C. J.; Frechet, J. M. J.; Turner, S. R. *Macromolecules* **1992**, *25*, 4583.
(8) Chu, F.; Hawker, C. J. *Polym. Bull*. **1993**, *30*, 265.
(9) Spindler, R.; Frechet, J. M. J. *Mcromolecules* **1993**, *26*, 4809.
(10) Mathias, L. J.; Carothers, T. *J. Am. Chem. Soc*. **1991**, *113*, 4043.
(11) Lach, C.; Muller, P.; Frey, H.; Mulhaupt, R. *Macromol. Rapid. Commun*. **1997**, *18*, 253.
(12) Hobson, L. J.; Feast, W. J. *Polymer* **1999**, *40*, 1279.
(13) Boogh, L.; Pettersson, B.; Japon, S.; Manson, J. A. E. *Proc. ICCM-10* **1995**, *26*, 4617.
(14) Zhang, Y.; Wada, T.; Sasabe, H. *Polymer* **1997**, *38*, 2893.
(15) Hawker, C. J.; Mackay, M. E.; Wooley, K. L; Frechet, J. M. J. *J. Am. Chem. Soc.* **1995**, *117*, 4409.
(16) Uppuluri, S.; Morrison, F. A.; Dvornic, P. R. *Macromolecules* **2000**, *33*, 2551.
(17) Sendijarevic, I.; McHugh, A. J. *Macromolecules* **2000**, *33*, 590.
(18) Suneel; Buzza, D. M. A.; Groves, D. J.; McLeish, T. C. B.; Parker, D.; Keeney, A. J.; Feast, W. J. *Macromolecules* **2002**, *35*, 9605.
(19) Frechet. J. M. J.; Hawker. C. J.; Gitsov. I.; Leon. J. W. *J. Macromol. Sci. Pure Appl. Chem*. **1996**, *A33*, 1399.
(20) Hobson, L. J.; Feast, W. J. *Chem. Commun.* **1997**, *21*, 2067.
(21) Mansfield, M. L.; Klushin, L. I. *J. Phys. Chem*. **1992**, *96*, 3994.
(22) Fixman, M. *J. Chem. Phys*. **1983**, *78*, 1588.
(23) Aerts, J. *Comput. Theor. Polym. Sci*. **1998**, *2*, 49.
(24) Widmann, A. H.; Davies, G. R. *Comput. Theor. Polym. Sci*. **1998**, *8*, 191.
(25) Lyulin, A. V.; Davies, G. R.; Adof, D. B. *Macromolecules* **2001**, *34*, 3783.
(26) Sheridan, P. F.; Adolf, D. B.; Lyulin, A. V.; Neelov, I. M.; Davies, G. R. *J. Chem. Phys*. **2002**, *117*, 7802.
(27) Frank, F. C.; Keller, A.; Mackley, M. R. *Polymer* **1971**, *12*, 467.
(28) *Flexible Polymer Chain Dynamics in Elongational Flow. Theory and Experiment*; Nguyen T. D., Kausch H. H., Eds.; Springer Verlag: Heidelberg, Germany, 1999.
(29) Perkins, T. T.; Smith, D. E.; Chu, S. *Science* **1997**, *276*, 2016.
(30) Smith, D. E.; Chu, S. *Science* **1998**, *281*, 1335.
(31) de Gennes, P. G. *J. Chem. Phys*. **1974**, *60*, 5030.

(32) Hinch, E. J. *Polymeres et lubrification, colloques internationaux du CNRS*; 1974; No. 233, p 241.
(33) Magda, J. J.; Larson, R. G.; Mackay, M. E. *J. Chem. Phys*. **1988**, *89*, 2504.
(34) López, C. J. J.; de la Torre, H.; García, J. *J. Chem. Phys*. **1991**, *95*, 9384. Cifre, J. G.; de la Torre, H.; García, J. *J. Rheol*. **1999**, *43*, 339.
(35) Agarwal, U. S.; Bhargava, R.; Mashelkar, R. A. *J. Chem. Phys*, **1998**, *108*, 1610. Agarwal, U. S.; Bhargava, R.; Mashelkar, R. A. **2000**, *113*, 3397.
(36) (a) Neelov, I.; Lyulin, A.; Davies, G. R.; Adolf, D. B. *J. Chem. Phys.* **2002**, *33*, 3294. (b) Neelov, I. M.; Adolf, D. B. *Macromolecules* **2003**, *36*, 6914.
(37) (a) Lee, A. T.; McHugh, A. J. *Macromol. Theory Simul*. **2001**, *10*, 244. (b) Lee, A. T.; McHugh, A. J. *Macromol. Theory Simul*. **2001**, *10*, 430.
(38) Lee, A. T.; McHugh, A. J. *Macromolecules* **2001**, *34*, 7127.
(39) Ermak, D. L.; McCammon, J. A. *J. Chem. Phys.* **1978**, *69*, 1352.
(40) Ottinger, H. C. *Stochastic Processes in Polymeric Fluids*; Springer-Verlag: New York, 1996; p 244.
(41) Rey, A.; Freire, J. J.; García de la Torre, J. *Macromolecules* **1987**, *20*, 2385.
(42) Rotne, J.; Prager, S. *J. Chem. Phys*. **1969**, *50*, 4831.
(43) Hölter, D.; Burgath, A.; Frey, H. *Acta Polym.* **1977**, *48*, 30.
(44) Wiener, H. *J. Am. Chem. Soc.* **1947**, *69*, 17.
(45) Rouvray, D. H. *Math. Chem. (MATCH)* **1975**, *1*, 125.
(46) Rouvray, D. H.; Crafford, S. S. *Afr. J. Sci.* **1976**, *72*, 47.
(47) Bonchev, D.; Mekenyan, O.; Kamenska, V. *Math. Chem. (MATCH)* **1992**, *11*, 107.
(48) Gutman, I.; Yeh, Y.-N.; Lee, S. L.; Luo, Y.-L. *Ind. J. Chem.* **1993**, *32A*, 651.
(49) Murat, M.; Grest, G. *Macromolecules* **1996**, *29*, 1278.